Article

Quantitative Analysis of Backbone Dynamics in a Crystalline Protein from Nitrogen-15 Spin–Lattice Relaxation

Nicolas Giraud, Martin Blackledge, Maurice Goldman, Anja Bckmann, Anne Lesage, Franois Penin, and Lyndon Emsley

J. Am. Chem. Soc., **2005**, 127 (51), 18190-18201• DOI: 10.1021/ja055182h • Publication Date (Web): 30 November 2005

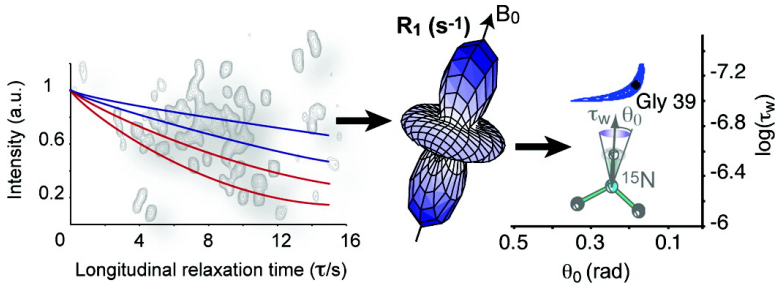

More About This Article

Additional resources and features associated with this article are available within the HTML version:

- Supporting Information
- Links to the 12 articles that cite this article, as of the time of this article download
- Access to high resolution figures
- Links to articles and content related to this article
- Copyright permission to reproduce figures and/or text from this article

View the Full Text HTML

J|A|C|S
ARTICLES
Published on Web 11/30/2005

Quantitative Analysis of Backbone Dynamics in a Crystalline Protein from Nitrogen-15 Spin−Lattice Relaxation

Nicolas Giraud,[†] Martin Blackledge,[‡] Maurice Goldman,[§] Anja Böckmann,[||] Anne Lesage,[†] François Penin,[||] and Lyndon Emsley*,[†]

Contribution from the Laboratoire de Chimie (UMR 5182 CNRS/ENS Lyon), Laboratoire de Recherche Conventionné du CEA (DSV 23V/DSM 0432), Ecole Normale Supérieure de Lyon, Lyon, France, Institut de Biologie Structurale Jean Pierre Ebel (CNRS/CEA/UJF), 41 rue Jules Horowitz, 38027 Grenoble, France, CEA Saclay, DSM/DRECAM/Service de Physique de l'Etat Condensé, F-91191 Gif sur Yvette, France, and Laboratoire de Conformation des Protéines (UMR 5086 IBCP/CNRS), Institut de Biologie et Chimie des Protéines, Lyon, France

Received July 30, 2005; E-mail: lyndon.emsley@ens-lyon.fr

Abstract: A detailed analysis of nitrogen-15 longitudinal relaxation times in microcrystalline proteins is presented. A theoretical model to quantitatively interpret relaxation times is developed in terms of motional amplitude and characteristic time scale. Different averaging schemes are examined in order to propose an analysis of relaxation curves that takes into account the specificity of MAS experiments. In particular, it is shown that magic angle spinning averages the relaxation rate experienced by a single spin over one rotor period, resulting in individual relaxation curves that are dependent on the orientation of their corresponding carousel with respect to the rotor axis. Powder averaging thus leads to a nonexponential behavior in the observed decay curves. We extract dynamic information from experimental decay curves, using a diffusion in a cone model. We apply this study to the analysis of spin−lattice relaxation rates of the microcrystalline protein Crh at two different fields and determine differential dynamic parameters for several residues in the protein.

1. Introduction

Determination of molecular dynamics is essential to structural studies of proteins, since internal motion is a fundamental modulator of structure−function relationships.[1] Solution state NMR,[2−4] as well as computer simulations,[5] supply a rich insight into fast motions of the protein backbone. So far, the widespread study of internal motions in solid protein samples has been limited by the lack of suitable experimental protocols.

Very recently solid state NMR methods have been developed which allow the study, at an atomic scale, of microcrystalline proteins in the solid state: high resolution MAS spectra recorded on fully labeled samples have led to complete structural[6−8] studies of model systems. In this context, carrying on from previous pioneering studies,[9−11] we have shown that it is possible to record individual longitudinal relaxation rates and obtain widespread, site-specific information about the variations in nitrogen-15 spin−lattice relaxation rates along the protein backbone.[12] Nitrogen-15 spins can be considered as local probes for the study of internal mobility in solid proteins.[9] We observed in the protein Crh that the qualitative analysis of relaxation rates allows for a possible distinction between flexible and more rigid parts of the backbone.[12]

In this article we present further development of the theoretical model initially proposed by Torchia and Szabo[9] to quantitatively determine fluctuations in local dynamics and distinguish between time scale and motional amplitude effects. Notably, we examine different averaging schemes in order to propose an analysis of relaxation curves that takes into account the specificity of magic angle spinning (MAS) experiments. In particular, we show that MAS averages the relaxation effects experienced by a single spin over one rotor period, resulting in individual relaxation curves that then depend on the orientation of the corresponding carousel angle with respect to the rotor axis. Powder averaging thus leads to a nonexponential behavior in the observed decay curves. Finally, we apply this study to the analysis of spin−lattice relaxation rates for the microcrystalline protein Crh at two different magnetic fields.

2. Theory

In this section we will develop a formalism to predict spin−lattice relaxation curves in powdered solids undergoing MAS.

[†] Ecole Normale Supérieure de Lyon.
[‡] Institut de Biologie Structurale Jean Pierre Ebel.
[§] CEA Saclay.
[||] Institut de Biologie et Chimie des Protéines.

(1) Rasmussen, B. F.; Stock, A. M.; Ringe, D.; Petsko, G. A. *Nature* **1992**, *357* (6377), 423−424.
(2) Lipari, G.; Szabo, A. *J. Am. Chem. Soc.* **1982**, *104*, 4546−4559.
(3) Akke, M.; Palmer, A. G. *J. Am. Chem. Soc.* **1996**, *118* (4), 911−912.
(4) Pellecchia, M.; Sem, D. S.; Wuthrich, K. *Nature Reviews Drug Discovery* **2002**, *1* (3), 211−219.
(5) Storch, E. M.; Daggett, V. *Biochemistry* **1995**, *34* (30), 9682−9693.
(6) Castellani, F.; van Rossum, B.; Diehl, A.; Schubert, M.; Rehbein, K.; Oschkinat, H. *Nature* **2002**, *420*, 98−102.
(7) Zech, S. G.; Wand, A. J.; McDermott, A. E. *J. Am. Chem. Soc.* **2005**, *127* (24), 8618−8626.
(8) Lange, A.; Becker, S.; Seidel, K.; Giller, K.; Pongs, O.; Baldus, M. *Angew. Chem.* **2005**, *44* (14), 2089−2092.
(9) Cole, H. B. R.; Torchia, D. *Chem. Phys.* **1991**, *158* (2−3), 271−281.
(10) Mack, J. W.; Usha, M. G.; Long, J.; Griffin, R. G.; Wittebort, R. J. *Biopolymers* **2000**, *53* (1), 9−18.
(11) Torchia, D.; Szabo, A. *J. Magn. Reson.* **1982**, *49*, 107−121.
(12) Giraud, N.; Böckmann, A.; Lesage, A.; Penin, F.; Blackledge, M.; Emsley, L. *J. Am. Chem. Soc.* **2004**, *126* (37), 11422−11423.

10.1021/ja055182h CCC: $30.25

We develop this model for dipolar relaxation due to sufficiently fast internal motions of the N−H bond vector, which places us within the limits of Redfield relaxation theory.[13,14] Many previous studies have used Redfield theory to predict relaxation properties in solids,[15−17] notably for deuterium. A particularly interesting study was carried out by Varner et al.,[18] where they considered carbon-13 relaxation times for the extreme narrowing limit, extending the work of Torchia and Szabo. In this article, we simply concentrate on an approach adapted to the problem at hand, which is valid for all time scales within the validity of Redfield theory.

2.1. Longitudinal Relaxation in Solids. We consider the amide group in a peptide bond and assume nitrogen-15 relaxation is due to the $^{15}N-^{1}H$ dipole−dipole coupling, neglecting the anisotropy of the chemical shift (which could be incorporated into the model). In this case the longitudinal relaxation rate (R_1) can be written[17]

$$R_1 = \frac{1}{T_1} = \frac{1}{4}\left(\frac{\gamma_H\gamma_N}{\langle r_{NH}\rangle^3}\frac{h}{2\pi}\right)^2 [J_0(\omega_H - \omega_N) + 3J_1(\omega_N) + 6J_2(\omega_H + \omega_N)] \quad (1)$$

where γ_N and γ_H are gyromagnetic ratios of ^{15}N and ^{1}H, h is Planck's constant, and $\langle r_{NH}\rangle$ is the effective $^{15}N-^{1}H$ distance (considering vibrational motions). For the calculations described herein, $\langle r_{NH}\rangle$ was set to 1.02 Å. Finally, $J_m(\omega)$ is a spectral density function defined as[13,14,19]

$$J_m(\omega) = 2\int_0^\infty G_m(t)\cos(\omega t)\,dt \quad (2)$$

where $G_m(t)$ is an autocorrelation function which depends on the nature of $^{15}N-^{1}H$ bond motion and the choice of the frame in which it is described. In the most simple case of a single orientation of a given N−H vector in a static sample of protein fixed in the laboratory frame, $G_m(t)$ is given by

$$G_m(t) = \langle Y_{2m}(\Theta(0))Y_{2m}^*(\Theta(t))\rangle, \quad (3)$$

where Y_{2m} are spherical harmonics and $\Theta(t)$ describes the orientation of the N−H vector[2] with respect to the laboratory frame. In the following we choose to assume that the $^{15}N-^{1}H$ bond dynamics is well described by free diffusion, with a diffusion constant D_w, within a cone of semiangle θ_0 (though we could choose other motional models; see section 3). We also assume that the protein molecule undergoes no overall tumbling (this is the principle difference with respect to solution state models for relaxation).

Although there is no analytical expression for $G_m(t)$ in the case of this diffusion in a cone model, Lipari and Szabo[20] have proposed time-dependent Padé approximants to correlation functions of second-order spherical harmonics within this motional model. Notably, whereas for a system in solution correlation functions do not depend on the order m of the spherical harmonics, in the solid state the absence of overall tumbling requires that we calculate individually $J_0(\omega)$, $J_1(\omega)$, and $J_2(\omega)$ in order to account for the molecular orientation dependence of relaxation rates with respect to the external magnetic field. The expressions for these autocorrelation functions are[11]

$$G_m(t) = G_m(\infty) + (G_m(0) - G_m(\infty))e^{-t/\tau_m^{eff}} \quad (4)$$

where

$$\tau_0^{eff} = \frac{x_0^2(1+x_0)^2\{\ln[(1+x_0)/2] + (1-x_0)/2\}/2(x_0-1)}{D_w(G_0(0) - G_0(\infty))} + \frac{(1-x_0)(2-x_0-9x_0^2-7x_0^3)}{60D_w(G_0(0) - G_0(\infty))}$$

$$\tau_{\pm1}^{eff} = \frac{(1-x_0)^2(9+32x_0+44x_0^2+20x_0^3)/120}{D_wG_{\pm1}(0)}$$

$$\tau_{\pm2}^{eff} = \frac{(1-x_0)^3(8+12x_0+5x_0^2)/240}{D_wG_{\pm2}(0)}$$

$$G_0(0) = \frac{1}{20}[x_0(1+x_0)(9x_0^2-1)+4]$$

$$G_{\pm1}(0) = \frac{1}{10}(1-x_0)[(2+x_0)(1+3x_0^2)+3x_0]$$

$$G_{\pm2}(0) = \frac{1}{40}(1-x_0)^2(3x_0^2+9x_0+8)$$

$$G_0(\infty) = \left[\frac{1}{2}x_0(1+x_0)\right]^2$$

$$G_{\pm1}(\infty) = G_{\pm2}(\infty) = 0$$

and $x_0 = \cos\theta_0$. The resulting single-exponential approximations for $G_m(t)$ are highly accurate for $0 < \theta_0 < 90°$ when $m = 0$, ±2 and for $0 < \theta_0 < 75°$ when $m = \pm1$ (which should be a reasonable range for more or less rigid residues in a crystalline system).

In magic angle spinning experiments, we need to consider that the sample is a powder composed of crystallites with an isotropic distribution of orientations in a rotor which is spinning about an axis oriented at the magic angle with respect to the magnetic field. Thus, the orientation of the N−H vector, responsible for relaxation, depends on the orientation of the crystallite and the instantaneous rotor position. We thus describe the time-dependent orientation of any given N−H vector through the following series of reference frames.[11] Diffusion in a cone is described by going from the principal axis coordinate system P to the crystal-fixed coordinate system C. The powder orientations are taken into account by going from C to a rotor fixed system M, and finally MAS is taken into account through rotation of M to the laboratory frame L. This series of reference frames is illustrated schematically in Figure 1.

(13) Redfield, A. G. *Advances in Magnetic Resonance*; Academic Press: New York, 1965; Vol. 1, p 1.
(14) Abragam, A. *The Principles of Nuclear Magnetism*; Clarendon Press: Oxford, 1961.
(15) Vold, R. R.; Vold, R. L. Deuterium Relaxation in Molecular Solids. In *Advances in Magnetic and Optical Resonance*; Warren, W. S., Ed.; Academic Press: New York, 1991; p 85.
(16) Wang, A. C.; Kennedy, M. A.; Reid, B. R.; Drobny, G. P. *J. Magn. Reson. B* **1994**, *105* (1), 1−10.
(17) Spiess, H. W. Rotation of Molecules and Nuclear Spin Relaxation. In *NMR Basic Principles and Progress*; Diehl, P., Fluck, E., Kosfeld, R. Springer-Verlag: Berlin, Heidelberg, New York, 1978; p 15.
(18) Varner, S. J.; Vold, R. L.; Hoatson, G. L. *J. Magn. Reson.* **2000**, *142* (2), 229−240.
(19) Bloembergen, N.; Purcell, E. M.; Pound, R. V. *Nature* **1947**, *160* (4066), 475−476.
(20) Lipari, G.; Szabo, A. *J. Chem. Phys.* **1981**, *75* (6), 2971−2976.

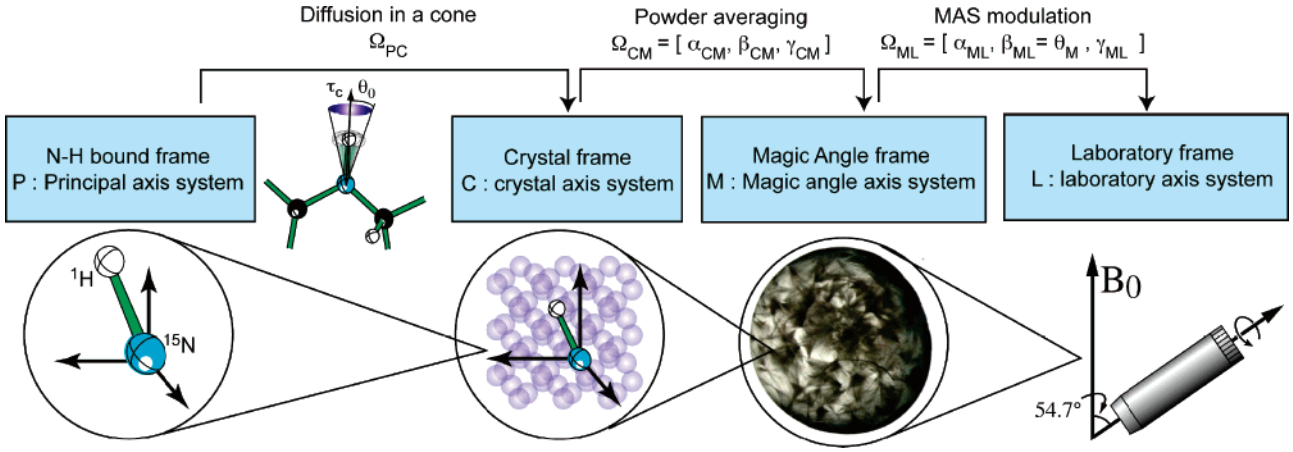

Figure 1. Reference frames used to describe nitrogen-15 relaxation. (The microscope view shows microcrystals of the protein Crh.[21,22])

With respect to this decomposition each autocorrelation function can be expressed in the laboratory frame as[11]

$$C_a(t) = \sum_{bb'=-2}^{2} \sum_{m=-2}^{2} D^{(2)}_{mb}{}^*(\Omega_{CM})\, D^{(2)}_{ba}{}^*(\Omega_{ML})\, D^{(2)}_{mb'}(\Omega_{CM}) \times D^{(2)}_{b'a}(\Omega_{ML}) \times G_m(t) \quad (5)$$

with ($a = 0, \pm1, \pm2$) and where $D^{(2)}_{ab}$ are Wigner rotation matrix elements[17] and $D^{(2)}_{ab}{}^*$ are the corresponding conjugate matrix elements. Rotations through Euler angles[23] $\Omega_{CM} = (\alpha_{CM}, \beta_{CM}, \gamma_{CM})$ and $\Omega_{ML} = (\alpha_{ML}, \beta_{ML}, \gamma_{ML})$ bring, respectively, the frame C into coincidence with the frame M and the frame M into coincidence with the frame L, as shown in Figure 1. $G_m(t)$ is the autocorrelation function expressed in the crystal frame C.[20]

Torchia and Szabo[11] proposed that, for a powder under MAS, the measured R_1 obtained from the initial slope of the relaxation curves can be described by a unique correlation function, obtained from double averaging of $G_m(t)$ over the powder and the rotor orientations, insofar as

$$\omega_r > \hbar \frac{\gamma_H \gamma_N}{r_{NH}^3} \frac{\mu_0}{4\pi}$$

(where ω_r is the rotor spinning speed (s^{-1})):

$$C_a(t) = C^{TS}(t) = \sum_{m=-2}^{2} G_m(t) \quad (6)$$

Note that while in solution calculations the autocorrelation function decays to zero due to overall tumbling, in solids where the motion is restricted $C^{TS}(t)$ does not decay to zero on a time scale relevant to Redfield theory. Nevertheless, since we are only interested in the fluctuating part of this function, for longitudinal relaxation we can legitimately only consider its Fourier transform for values $\omega \neq 0$ without introducing any errors. (Note that this is not the case for transverse relaxation rates.)

2.2. Orientation and Time Dependence of Longitudinal Relaxation in Solids. The double averaging approach was particularly useful in the absence of powerful computers, since it provided a simple orientation-independent single-exponential expression for T_1 that was easy to evaluate. In the following we propose an "explicit averaged sum" (EAS) approach to calculating the relaxation curves that accounts for the orientation dependence of the relaxation rates and can today be easily evaluated.

A longitudinal relaxation curve is the sum of signals from molecules in all the crystallites making up the powder, each of them being a priori modulated by MAS. We can thus distinguish two kinds of angular dependence for $C_a(t)$. First, in each single crystallite, the relaxation rate is modulated by the variation of α_{ML} from 0 to 2π due to sample rotation. Second, the crystallite orientation dependence is described through variations of β_{CM} (from 0 to π) and γ_{CM} (from 0 to 2π). In this way, the $C_a(t)$ appear as a linear combination of orientation and time dependent terms:

$$C_a(t) = \sum_{bb'=-2}^{2} \sum_{m=-2}^{2} D^{(2)}_{mb}{}^*(\Omega_{CM})\, D^{(2)}_{mb'}(\Omega_{CM})\, D^{(2)}_{ba}{}^*(\Omega_{ML}(t)) \times D^{(2)}_{b'a}(\Omega_{ML}(t)) \times G_m(t) \quad (7)$$

Figure 2 shows the orientation dependence of the longitudinal relaxation rate for a nitrogen-15 nucleus bound to a proton, without magic angle spinning, which diffuses in a cone with a diffusion time $\tau_w = 1/6D_w = 6.6 \times 10^{-8}$ s and semiangle θ_0 of 11.2° and 45°, respectively. We can see that in fact the relaxation rate, R_1^{cryst}, is strongly anisotropic. It is faster when the interaction vector is either parallel to the external magnetic field or perpendicular to it and is slow when the vector is oriented at the magic angle with respect to the field. Furthermore, when the motion is less restricted, we observe that the relaxation rate becomes less sensitive to the orientation of the $^{15}N-^1H$ bond.

In addition to the anisotropy of the relaxation rate shown in Figure 2, for a given orientation of the interaction vector in the rotor, a modulation due to MAS of the relaxation rate can also be expected. Figure 3 shows the variations of R_1^{cryst} with respect to the orientation of the $^{15}N-^1H$ bond in the rotor: we note that rotor position can be varied through either γ_{CM} or α_{ML}, which are equivalent (indeed, henceforth we will only refer to γ_{CM}, except in eq 14, where it is more logical to use α_{ML}). From this figure, we can see that, for a given β_{CM}, a ^{15}N spin will

(21) Böckmann, A.; Lange, A.; Galinier, A.; Luca, S.; Giraud, N.; Juy, M.; Heise, H.; Montserret, R.; Penin, F.; Baldus, M. *J. Biomol. NMR* **2003**, *27* (4), 323−339.
(22) Juy, M.; Penin, F.; Favier, A.; Galinier, A.; Montserret, R.; Haser, R.; Deutscher, J.; Böckmann, A. *J. Mol. Biol.* **2003**, *332*, 767−776.
(23) Rose, M. E. *Elementary Theory of Angular Momentum*; John Wiley: New York, 1957.

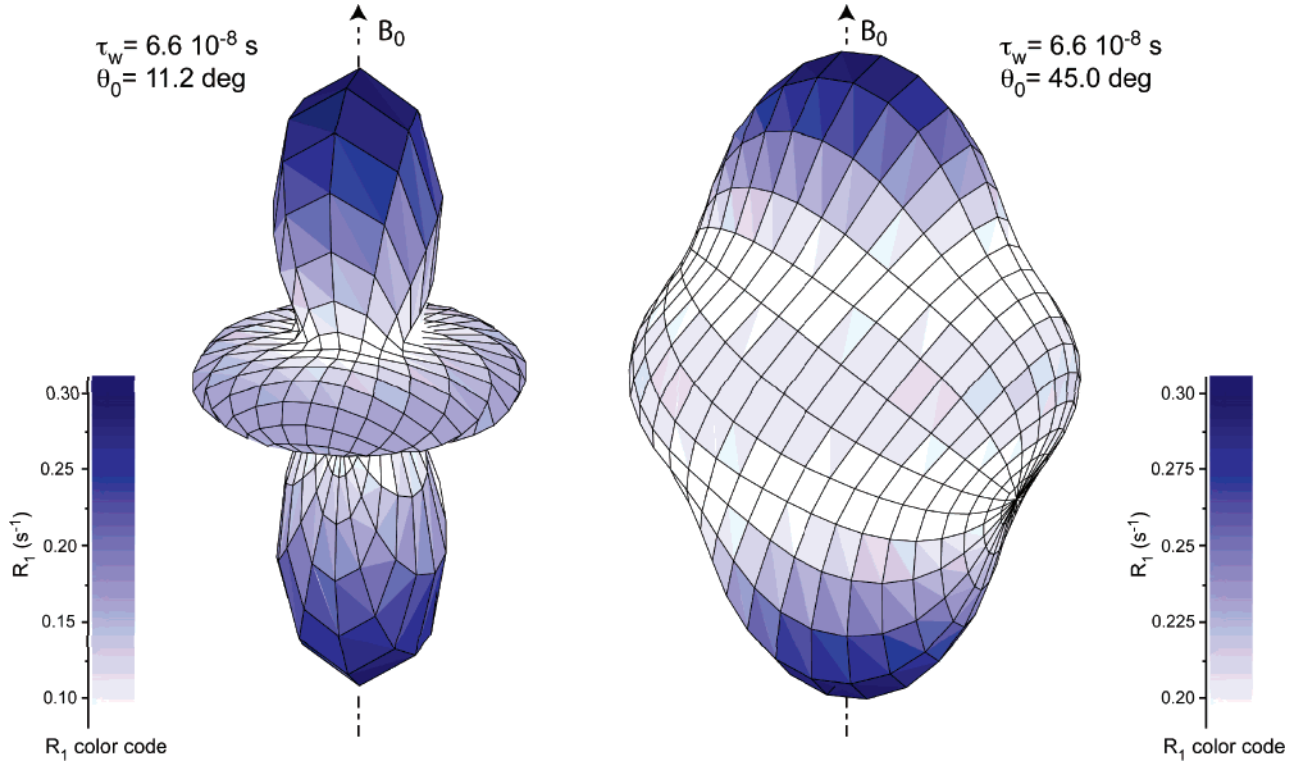

Figure 2. Orientation dependence of nitrogen-15 longitudinal relaxation rate. R_1^{cryst} is plotted for two motional amplitudes ($\theta_0 = 11.2°$ and 45°), in spherical coordinates as a function of the orientation of the $^{15}N-^{1}H$ bond with respect to the external magnetic field B_0. The interaction vector is wobbling with a diffusion time $\tau_w = 1/6D_w = 6.6 \times 10^{-8}$ s. Relaxation rates are calculated for a 500 MHz proton frequency. The figure is shown color coded with respect to the value of R_1^{cryst} for each amplitude (note that the color codes goes from the maximum to the minimum relaxation rates for both models and are slightly different).

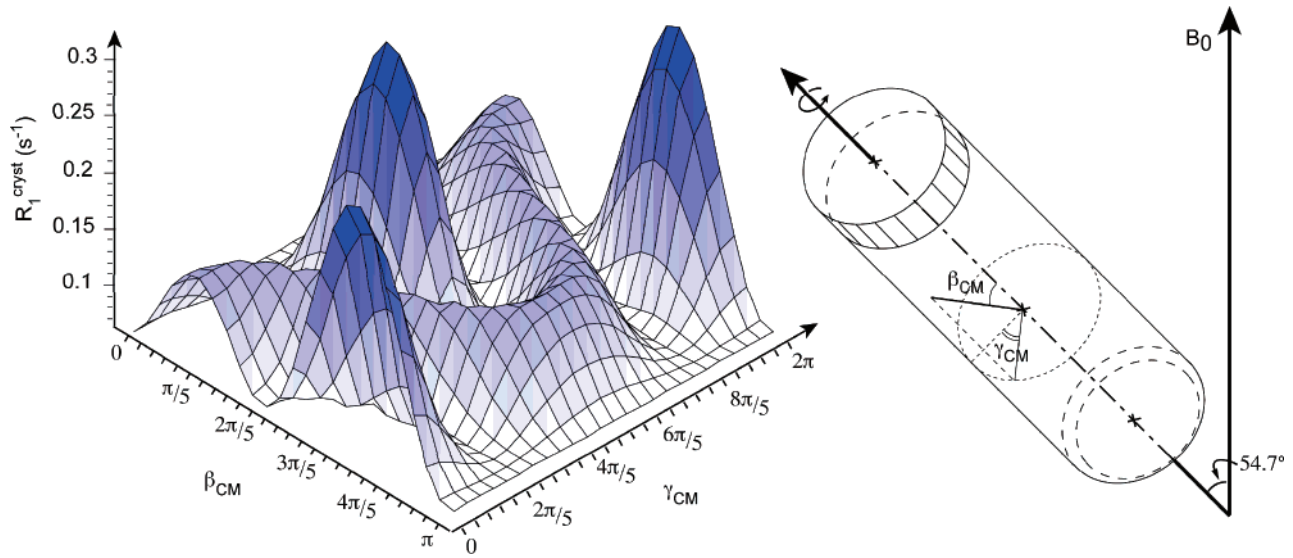

Figure 3. Dependence of nitrogen-15 longitudinal relaxation rate on orientation of $^{15}N-^{1}H$ bond in the rotor frame: the $^{15}N-^{1}H$ bond is assumed to wobble with a diffusion time $\tau_w = 1/6D_w = 6.6 \times 10^{-8}$ s in a cone of semiangle $\theta_0 = 11.2°$. R_1^{cryst} is calculated from eq 1, using autocorrelation functions $C_a(t)$ from eq 7, for a 500 MHz proton frequency.

undergo a time-dependent relaxation rate as γ_{CM} varies over a rotor period.

If we consider a carousel[24] of $^{15}N-^{1}H$ bonds having the same β_{CM} angle, their orientations can be interchanged by a rotation about the spinning axis, and so each of them will undergo the same overall modulation of R_1^{cryst} over a rotor period which is shown in Figure 4a. Figure 4b then shows the relaxation curves calculated either for a crystallite undergoing slow MAS or for the same crystallite undergoing the corresponding average relaxation rate. Both curves are numerical solutions to the modified Bloch equation for longitudinal relaxation[25]:

$$\frac{d(M_z(t) - M_z^0)}{dt} = -R_{1[\alpha_{ML}(t)]}(M_z(t) - M_z^0) \qquad (8)$$

where $M_z(t)$ is the nitrogen-15 longitudinal magnetization and

(24) Antzutkin, O. N.; Song, Z. Y.; Feng, X. L.; Levitt, M. H. *J. Chem. Phys.* **1994**, *100* (1), 130−140.

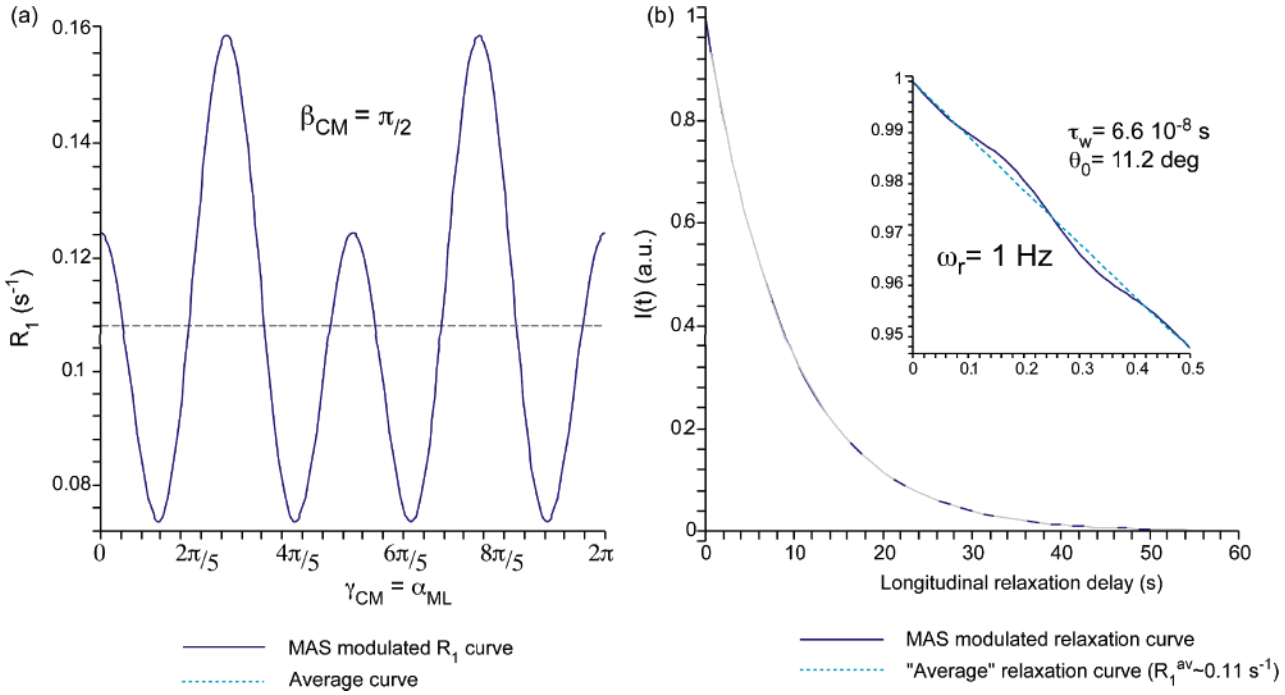

Figure 4. (a) Modulation of nitrogen-15 R_1^{cryst} as a function of rotor position (solid blue line), for a crystallite making an angle $\beta_{CM} = \pi/2$ with respect to the rotor axis, compared to the nitrogen-15 R_1 averaged over the rotor position for the same crystallite (dashed gray line). The ^{15}N relaxation rate is calculated for a ^{15}N−^{1}H bond with the same parameters as those for Figure 3. (b) Simulated relaxation curves for a nitrogen-15 nucleus undergoing modulated R_1^{cryst} (solid blue line) and for the same nitrogen-15 undergoing the single average R_1 (dashed gray line). The rotor spinning speed is 1 Hz.

M_z^0 the initial magnetization. Initial conditions are set such that $(M_z(t = 0\text{ s}) - M_z^0) = 1$.

The curve resulting from MAS modulation fluctuates around the "average" relaxation curve that would be expected for relaxation with an R_1 averaged over the rotor phase. Even at a rotor frequency of 1 Hz, the fluctuation is very weak on the time scale of the relaxation curve, and it becomes negligible at higher spinning speeds. As a result, we can assume that, for a given carousel (defined by β_{CM}), each crystallite undergoes an averaged R_1:

$$R_1^{MAS}(\beta_{CM}) = \frac{1}{2\pi}\int_{\alpha_{ML}=0}^{2\pi} R_1^{cryst}(\gamma_{CM}, \beta_{CM})\, d\gamma_{CM} \qquad (9)$$

2.2.1. Validity of the Averaging Scheme. Note that a priori we would imagine that the approach to handling the time dependence introduced by magic angle spinning is valid if (i) this time dependence is much shorter than relaxation times T_1 and T_2: $\omega_r T_{1,2} \gg 1$ and (ii) it is much longer than the correlation time τ_C: $\omega_r \tau_C \ll 1$. Interestingly, we find that condition (ii) is in fact not necessary, as follows. In this scheme, in addition to a periodic variation due to the passage to the interaction frame with frequencies $\pm\omega_L$, $\pm 2\omega_L$, some of the random interaction terms also experience a periodic fluctuation due to the rotation of the sample, with frequencies $\pm\omega_r$, $\pm 2\omega_r$. For such terms the correlation function has a periodic and random evolution of the form

$$G(t) = e^{[i(p\omega_L + q\omega_r) - 1/\tau_C]t}. \qquad (10)$$

This yields a spectral density

$$J(p\omega_L + q\omega_r) = \frac{\tau_C}{1 + (p\omega_L + q\omega_r)^2\tau_C^2}. \qquad (11)$$

The spinning frequency is in practice much lower than the Larmor frequency, and in general only terms with $p = 0$ can give results that are significantly sensitive to rotation. Therefore, there is no significant contribution of this type to longitudinal relaxation. Moreover, these terms correspond to secular dipolar terms with respect to the Zeeman interaction and would not therefore contribute to transverse relaxation. The resulting line broadening should not be visible on the residual line width under MAS. One case where the sample could be sensitive to the spinning frequency is the study of transverse relaxation under radio frequency fields. In this case, frequencies $\pm\omega_1$, $\pm 2\omega_1$ due to passage to the doubly rotating frame should be taken into account. One other case is the study of cross relaxation between spins with close resonance frequencies ($p \neq 0$), where we would have $\omega_L^i - \omega_L^j = \omega_r$. Thus eq 9 is validated.

2.3. Evaluation of Spectral Densities. $R_1^{MAS}(\beta_{CM})$ can also be expressed as a function of the spectral densities $J_i^{MAS}(\omega)$ which result from the same average over rotor positions:

$$R_1^{MAS}(\beta_{CM}) = \frac{1}{4}\left(\frac{\gamma_H\gamma_N}{\langle r_{NH}\rangle^3}\frac{h}{2\pi}\right)^2 [J_0^{MAS}(\omega_H - \omega_N) + 3J_1^{MAS}(\omega_N) + 6J_2^{MAS}(\omega_H + \omega_N)] \qquad (12)$$

where

$$J_i^{MAS}(\omega) = \frac{1}{2\pi}\sum_{j=-2}^{2} C_{ij}^{MAS}(\beta_1) \times \frac{[G_j(0) - G_j(\infty)]\tau_i^{eff}}{1 + (\omega\,\tau_j^{eff})^2} \qquad (13)$$

each $C_{ij}^{MAS}(\beta_1)$ is expressed as follows:

$$C_{ij}^{MAS}(\beta_1) = \sum_{bb'=-2}^{2} \{D_{jb}^{(2)*}(\Omega_{CM})\, D_{jb'}^{(2)}(\Omega_{CM}) \times [\int_{\alpha_{ML}=0}^{2\pi} D_{bi}^{(2)*}(\Omega_{ML})\, D_{b'i}^{(2)}(\Omega_{ML})\, d\alpha_{ML}]\} \quad (14)$$

To handle exact spectral densities and thus evaluate rigorously relaxation curves resulting from a powder, we have further developed these expressions using the Maple software.[26] $C_{ij}^{MAS}(\beta_1)$ is of the form

$$C_{ij}^{MAS}(\beta_1) = c_{ij}^{0} + c_{ij}^{I}\cos(\beta_1) + c_{ij}^{II}\cos^2(\beta_1) + c_{ij}^{III}\cos^3(\beta_1) + c_{ij}^{IV}\cos^4(\beta_1) \quad (15)$$

The computation of the c_{ij}^{λ} coefficients leads to numerical expressions that are detailed in the Supporting Information.

The nitrogen-15 longitudinal relaxation rate still depends on the orientation of the $^{15}N-^{1}H$ bond in the powder through β_{CM}. Figure 5a shows variations of R_1^{MAS} within the powder, under MAS. The signal acquired during a relaxation experiment is the sum of contributions from all orientations. Three cases may be considered. The first is the signal resulting from the orientation weighted explicit sum of relaxation curves for each value of β_{CM} in the powder under MAS (that we refer to as the "explicit averaged sum (EAS)," which can be obtained from eq 9 to be

$$I^{\exp}(t) = I_0^{\exp}\frac{\int_{\beta_{CM}=0}^{\pi} \exp[-R_1^{MAS}(\beta_{CM})t]\sin(\beta_{CM})\, d\beta_{CM}}{\int_{\beta_{CM}=0}^{\pi}\sin(\beta_{CM})\, d\beta_{CM}} \quad (16)$$

This is compared with the decaying curve explicitly evaluated for a static powder from eq 6:

$$I^{static}(t) = I_0^{static}\frac{\int_{\gamma_{CM}=0}^{2\pi}\int_{\beta_{CM}=0}^{\pi} \exp[-R_1^{cryst}(\gamma_{CM},\beta_{CM})t]\sin(\beta_{CM})\, d\beta_{CM}\, d\gamma_{CM}}{\int_{\gamma_{CM}=0}^{2\pi}\int_{\beta_{CM}=0}^{\pi}\sin(\beta_{CM})\, d\beta_{CM}\, d\gamma_{CM}} \quad (17)$$

Finally we compare this with the model from Torchia and Szabo[11] of a single-exponential curve whose relaxation rate is given by

$$I^{initial-slope}(t) = I_0{}^{is}\exp[-R_1^{TS}t], \quad (18)$$

Note that R_1^{TS} in eq 18 is defined as follows:[11]

$$R_1^{TS} = \frac{1}{T_1} = \frac{1}{4}\left(\frac{\gamma_H\gamma_N}{\langle r_{NH}\rangle^3}\frac{h}{2\pi}\right)^2 [J^{TS}(\omega_H-\omega_N) + 3J^{TS}(\omega_N) + 6J^{TS}(\omega_H+\omega_N)] \quad (19)$$

where $J^{TS}(\omega)$ is the Fourier transform of $C^{TS}(t)$ introduced in eq 6:

$$J^{TS}(\omega) = 2\int_0^{\infty} C^{TS}(t)\cos(\omega t)\, dt \quad (20)$$

We can see that formally this is equivalent to expressing R_1^{TS} as a powder average of local relaxation rates R_1^{cryst}:

$$R_1^{TS} = \frac{\iint_{\substack{\gamma_{CM}=0;2\pi\\ \beta_{CM}=0;\pi}} R_1^{cryst}[\beta_{CM},\gamma_{CM}]\sin(\beta_{CM})\, d\beta_{CM} d\gamma_{CM}}{\iint_{\substack{\gamma_{CM}=0;2\pi\\ \beta_{CM}=0;\pi}} \sin(\beta_{CM})\, d\beta_{CM}\, d\gamma_{CM}} \quad (21)$$

Finally, we remark that in order to calculate (and fit) inversion recovery curves, we can evaluate discrete sums for eqs 16 and 17 to obtain

$$I^{\exp}(t) \approx I_0^{\exp} \times \frac{\sum_{b=0}^{N_\beta-1}\exp\left[-R_1^{MAS}\left(\frac{(b+0.5)\pi}{N_\beta}\right)t\right]\sin\left(\frac{(b+0.5)\pi}{N_\beta}\right)}{\sum_{b=0}^{N_\beta-1}\sin\left(\frac{(b+0.5)\pi}{N_\beta}\right)} \quad (16a)$$

and

$$I^{static}(t) \approx I_0^{static} \times \frac{\sum_{a=0}^{N_\gamma-1}\sum_{b=0}^{N_\beta-1}\exp\left[-R_1^{cryst}\left(\frac{2a\pi}{N_\gamma},\frac{(b+0.5)\pi}{N_\beta}\right)t\right]\sin\left(\frac{(b+0.5)\pi}{N_\beta}\right)}{N_\gamma\sum_{b=0}^{N_\beta-1}\sin\left(\frac{(b+0.5)\pi}{N_\beta}\right)} \quad (17a)$$

respectively, where N_γ and N_β are the number of discrete powder angles used in the sum.

Figure 5b shows simulations of the decaying curves that would be recorded from a powder under MAS, according to our model of eq 16a, and from a powder without MAS (eq 17a) and the exponential curve calculated from R_1^{TS} for the same dynamics (eq 18). We note that, in the first two cases, using the explicit sum and averaged-sum models, these curves are nonexponential. Second, it is apparent that MAS significantly alters the relaxation curve as compared to the case of a static powder, for the same dynamics. Third, we see that the difference between the relaxation curve calculated with our explicit averaged sum (EAS) and the exponential approximation model, which is designed to be the best fit to the initial slope of the exact curve, is actually quite small. Figure 6 shows the difference between relaxation rates calculated using the single-exponential model (eq 18) and those obtained by fitting curves calculated using the EAS model (eq 16a) to a single-exponential function. The difference is plotted as a function of the diffusion time constant and the semiangle of the cone. This figure illustrates the degree of error that would be induced by not using the EAS model. For very rapid motions, at this field strength, we see that the error can be of the order of 20% of the measured relaxation rate.

In conclusion, we see that the EAS model developed here provides a more accurate prediction of relaxation rates and that

(25) Solomon, I. *Phys. Rev.* **1955**, *99* (2), 559−565.
(26) Maplesoft *Maple*, 9.50; 2004.

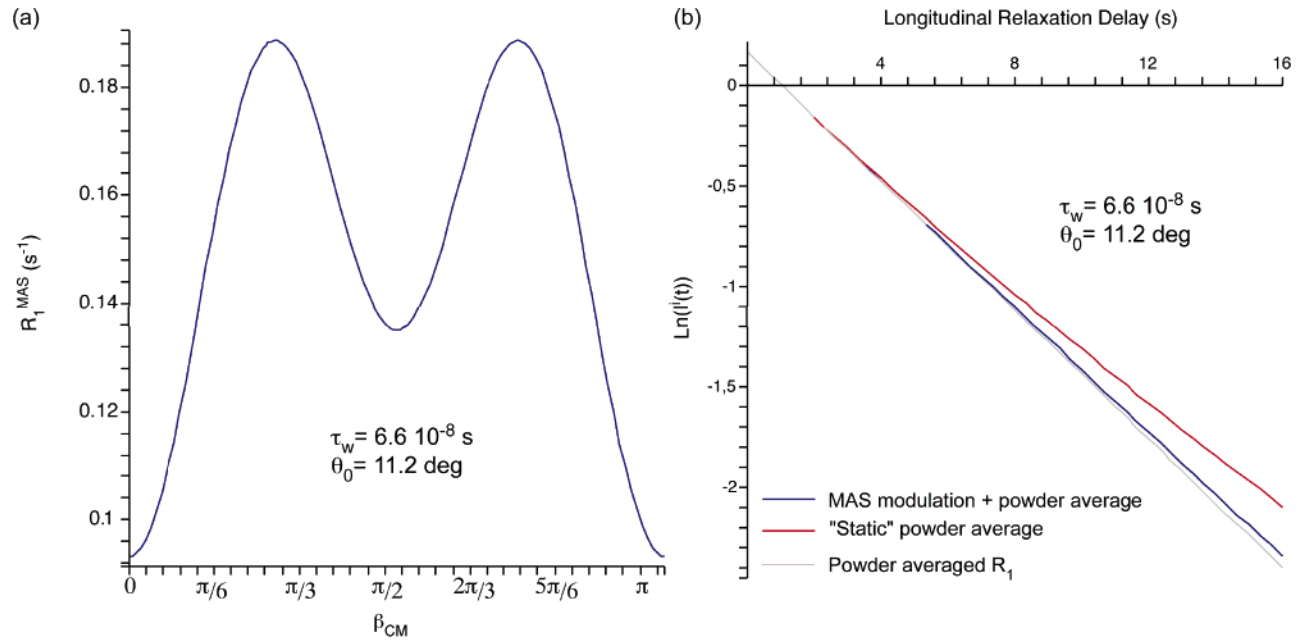

Figure 5. (a) Modulation of nitrogen-15 R_1^{MAS} as a function of β_{CM}, calculated with the same parameters as those for Figure 3. (b) Simulated nitrogen-15 relaxation curves for a powder undergoing MAS (blue), for a static powder (red), and an exponential curve corresponding to the initial slope of the relaxation curve of a powder under MAS (grey).

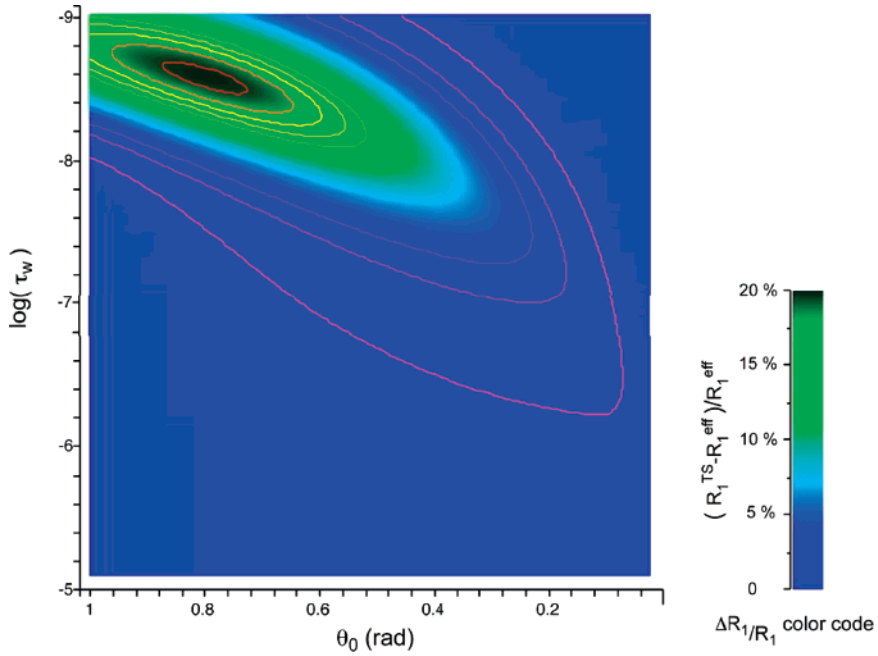

Figure 6. Plot of $\Delta R_1/R_1 = (R_1^{TS} - R_1^{eff})/R_1^{eff}$ as a function of $^{15}N-^{1}H$ bond dynamics. R_1^{eff} is calculated by least-squares fitting of the simulated (nonexponential) relaxation curve calculated for a powder under MAS using a monoexponential function, over the same time range (15 s) as that for which the corresponding experiments were carried out. R_1^{TS} is calculated using eq 18. Each relaxation rate is calculated at a 500 MHz proton frequency.

in certain cases significant errors could be induced by using the simplified model. We propose therefore to determine dynamic parameters from relaxation curves by simulating the full powder MAS dependence as given by eq 16 above.

We note that since an informative dynamic model uses at least two parameters to describe the motion (as is the case for the diffusion in a cone model used here (amplitude and rate)), it is of course impossible to determine the motion from a single relaxation measurement. Many strategies have been proposed in the literature, for both solids and liquids, to address this problem. In the following section we evaluate the field dependence of nitrogen-15 longitudinal relaxation in powders as a potential method to better define the dynamic parameters, and we show experimental results at two fields.

3. Magnetic Field Dependence of Longitudinal Relaxation Rates

As an indicator of field dependence, Figure 7 shows a contour plot of R_1^{eff} extracted by fitting curves calculated using eq 16, for a proton frequency of 500 MHz, as a function of the amplitude and the rate of the motion. Before continuing, we remark that the value of the diffusion time (τ_w), at which R_1^{eff} is

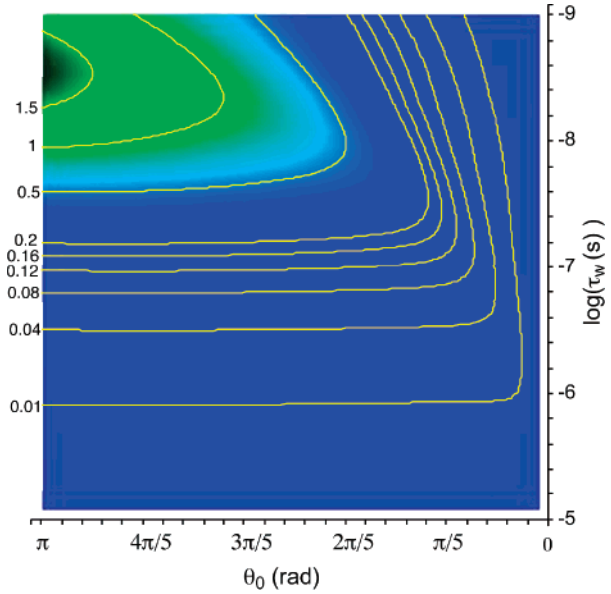

Figure 7. Plot of the effective longitudinal relaxation rate, R_1^{eff} as a function of $^{15}N-^{1}H$ bond dynamics (R_1^{eff} is calculated by least-squares fitting with a monoexponential function of the simulated nonexponential relaxation curve from a powder under MAS, simulated over a range of 15 s for a proton frequency of 500 MHz). For each dynamics, the relaxation curve was simulated on a 16 s relaxation delay from a distribution of 14 equally distributed values of β_{CM}, using numerical expressions for $R_1^{MAS}(\beta_{CM})$ according to EAS. R_1^{eff} was then calculated by fitting the simulated relaxation curve from 2 points (at 1 and 15 s, which is a compromise in order to estimate R_1^{eff} with accuracy, while optimizing computation time), resulting in a plot with 200 points in the diffusion time dimension, and 125 points in the cone-angle dimension.

the fastest, depends on the motional amplitude (θ_0). We note that this is in fact purely due to the way in which τ_w is defined in this triple exponential model for the correlation function. If we replot these data using an approximate single-exponential model, we find that the position of the maximum rate no longer depends on θ_0. This latter case is reminiscent of what would be expected from a model-free analysis, which by nature assumes a single-exponential correlation function (the full calculation of the model free version of this approach to relaxation in solids is under way in our laboratory).

In Figure 8, we show the magnetic field dependence of spin−lattice relaxation rates as calculated using the procedure described above. We note that the difference in rates between 11.74 and 16.45 T varies with the parameters of the dynamics assumed for the interaction vector but that, for motions in the time scale that is probably of relevance, we expect a measurable difference in relaxation rates, and thus we propose to use this difference to constrain experimentally the model.

4. Experimental Determination of Motional Parameters from Longitudinal Relaxation Curves

In a previous communication[12] we presented measurements of nitrogen-15 nuclear longitudinal relaxation rates in a microcrystalline sample of the protein Crh at 11.74 T. Here we use the same experiment to measure ^{15}N R_1's at 16.45 T and propose a procedure to extract a quantitative estimation of the $^{15}N-^{1}H$ bond motion along the protein backbone, using the diffusion in a cone model. Furthermore, we present an error analysis of our experimental data through indirect determination of standard deviations in R_1 at both fields.

Figure 9a shows the pulse sequence used to measure site specific R_1's from triple-resonance 2D $^{15}N-^{13}C$ correlation spectra (the pulse sequence and phase cycle are available on our web site[27] or upon request). The principle of this sequence is described elsewhere.[12] Experiments were run under the same conditions as those recorded at 500 MHz, and we obtained N-COCA correlation spectra under Cosine Modulated (CM) heteronuclear decoupling.[28−30]

Figure 9b shows a typical 2D spectrum ($\tau = 1$ s) for Crh. From these spectra, we could obtain unambiguously relaxation data from 31 resolved $^{15}N-^{13}C$ cross-peaks (assignment[21] shown on spectrum) and compare relaxation rates at both 11.74 and

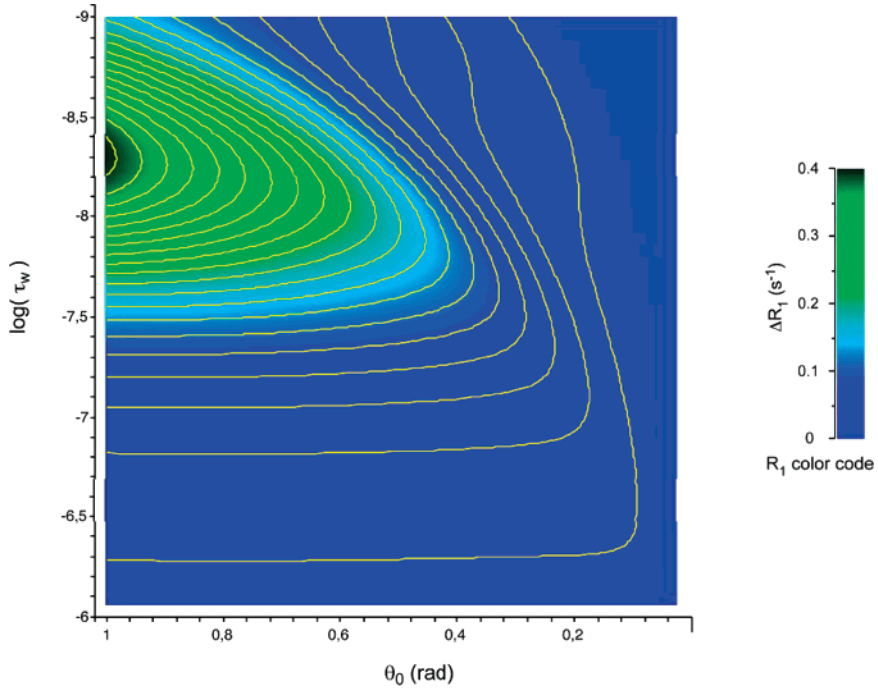

Figure 8. Difference between relaxation rates at 11.74 and 16.45 T. The parameters were the same as those for Figure 7.

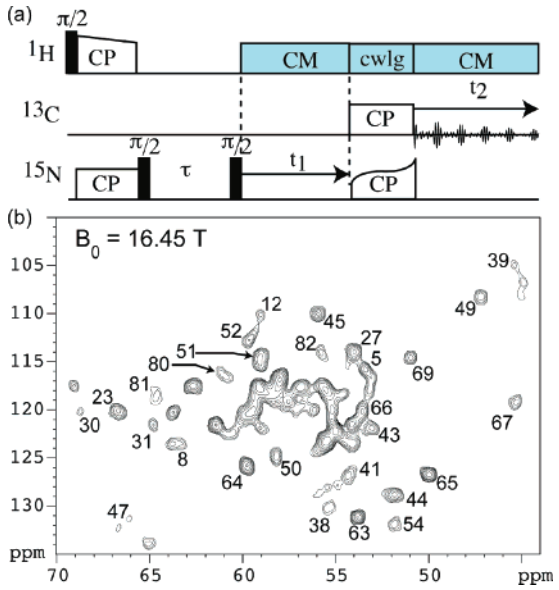

Figure 9. (a) The pulse sequence used to record the nitrogen-15 carbon-13 correlation spectra, resulting in spectra of the type shown in (b) for Crh at 16.45 T. The $^{1}H-^{15}N$ CP step was performed using a linear ramp (100% to 70% of r.f. field strength) on the ^{1}H channel, with a 1.7 ms CP period and an r.f. field strength of 50 kHz for ^{15}N. The 7 ms $^{15}N-^{13}C$ cross-polarization step used an adiabatic amplitude modulated tangential ramp on the nitrogen channel with r.f. field strengths of about 62 kHz and 50 kHz for ^{13}C and ^{15}N. The r.f. field strengths for the 90° pulses were 80 kHz for ^{1}H and 50 kHz for ^{15}N. The proton decoupling field was set to 80 kHz for CM and CWLG. Quadrature detection was obtained with TPPI. Each of the 375 increments in t_1 were acquired with 48 scans and a 3 s recycle delay between scans, with maximum acquisition times of 12.5 ms in t_1 and 16.6 ms in t_2. Data were processed using zero-filling up to 1024 points in t_1, 4096 points in t_2, a square cosine filter, and automatic baseline correction in both dimensions. The $\tau = 1$ s spectrum was recorded in 20 h, using about 6 mg of protein. Assignments are indicated according to Böckmann et al.[21]

16.45 T for 29 residues. Experiments were carried out on a Bruker Avance 700 MHz spectrometer using a 3.2 mm triple tuned CPMAS probe, at a spinning speed of 12 kHz, on a microcrystalline, uniformly labeled [^{15}N, ^{13}C] sample of the protein Crh in its domain swapped dimeric form (2 × 10.4 kDa).[21,22,31] The probe temperature was set to −7 °C, which corresponds to an effective sample temperature of about +8 °C. A series of spectra, with τ delays of 1, 14, and 7 s, respectively, were recorded using the same renormalization procedure as reported at 500 MHz.[12] R_1 data were then analyzed from peak intensities. (See Supporting Information for further details.)

Figure 10 shows typical decay curves measured for Asp 38 and Asp 69 at both fields. The accuracy of the evaluation of the spectral densities depends critically on the measured error in R_1, which has several potential sources. First, despite renormalization, the length of the experiments often leads to a slight detuning of the probe and an inhomogeneous change in intensity over the spectra due to cross polarization steps that cannot be perfectly compensated. Second, it appears that during the first few seconds of the decay curves, spin−lattice relaxation is not the only phenomenon that causes evolution of magnetization along the external magnetic field and that we have to account for a re-equilibration of magnetization between nearest neighbor nitrogens through spin diffusion, which causes an additional dispersion in observed relaxation rates. This effect will be considered in detail in a future article.

Although it is experimentally unreasonable to obtain a significant statistical ensemble of measurements so as to calculate the standard deviations, we can estimate that the distribution of peak intensities is the same for each measured point of the curve and is mainly due to noise. We assume that this distribution is normal, and we estimate its standard deviation σ to be 7.5% of the intensity at $\tau = 1$ s for each decay curve. The experimental curves are then fitted to a single-exponential decay curve with two parameters (initial intensity and relaxation rate), and we calculate the standard deviation of each measured rate by running a Monte Carlo simulation assuming that the simulated intensities for the best fit are at the center of a distribution.

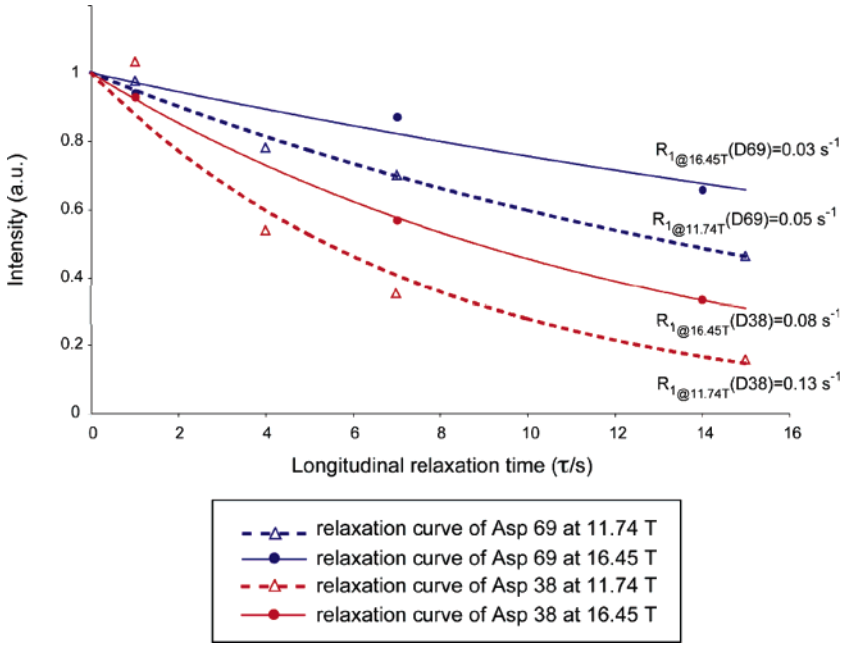

Figure 10. Decay curves measured at 16.45 T using three values of the relaxation delay τ, and which have been renormalized so that the initial intensities of the best fit curves are equal, compared to curves recorded at 11.74 T,[12] for Asp 38 and Asp 69.

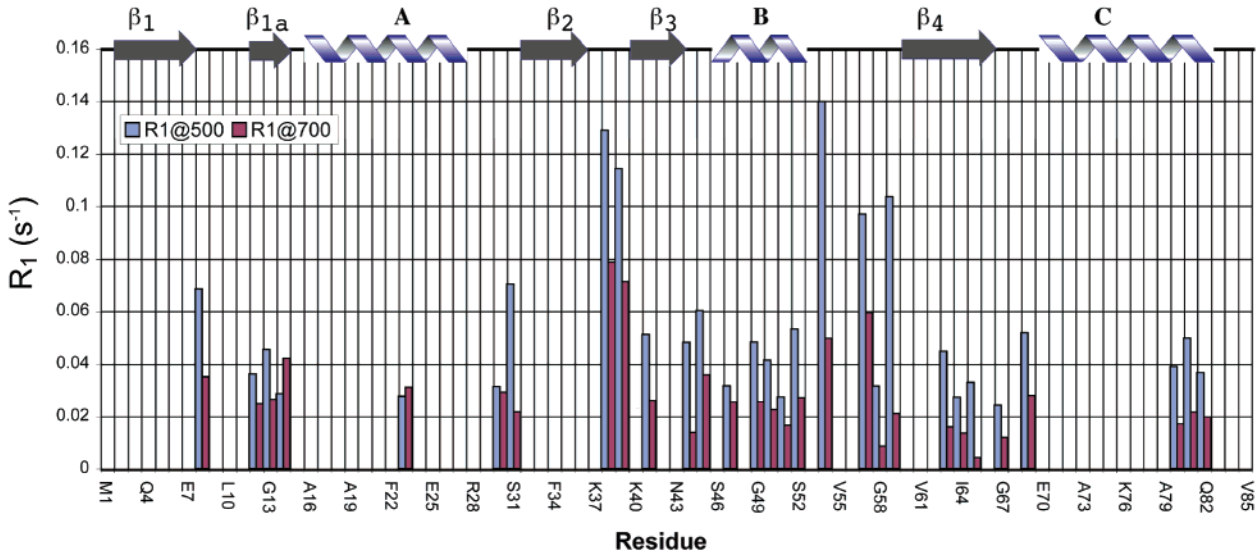

Figure 11. A bar graph of measured best fit R_1 vs residue number obtained from experiments using the sequence of Figure 11a, at 16.45 T (red) and 11.74 T (blue).

5. Results and Discussions

Figure 11 shows the best fit single exponential R_1 values measured for Crh (numerical values and standard deviations are given in the Supporting Information). First as expected from the previously reported data at 500 MHz,[12] we observe a qualitative correlation between relaxation rate and expected internal mobility for R_1 measured at 700 MHz.

We are now in a position to estimate for each residue the probability of a diffusion time τ_w and a cone angle θ_0 for the $^{15}N-^{1}H$ bond assuming diffusion in a cone. From the theoretical study above, we calculate $R_1^{eff}[\tau_c,\theta_0]$ by fitting the curve calculated using eq 9 to a single exponential function which we then compare to the fit values obtained from the data at both fields. (Note that we could also directly compare the predicted intensities in the curves with the data points.) We assume now that each relaxation rate R_1^{exp} that is determined from experiment is at the center of a normal distribution as defined in eq 22:

$$g(R_1, R_1^{exp}) = \frac{1}{\sigma\sqrt{2\pi}} \exp\left[\frac{-(R_1 - R_1^{exp})^2}{2\sigma^2}\right] \qquad (22)$$

where σ is the standard deviation, and R_1^{exp}, the center of the normal distribution. The probability for a given ^{15}N having the experimental relaxation rate R_1^{exp}, to wobble with a diffusion time τ_w and a cone angle θ_0, is proportional to

$$P_{[R_1^{exp}]}(\tau_c,\theta_0) \propto g(R_1^{eff}[\tau_c,\theta_0],R_1^{exp}) \qquad (23)$$

Hence, the probability for a ^{15}N with experimentally determined longitudinal relaxation rates $R^{exp}_{1[11.74T]}$ and $R^{exp}_{1[16.45T]}$, to diffuse in a cone of semi-angle θ_0, with a diffusion time τ_w is proportional to

$$P(\tau_c, \theta_0) = P_{[R^{1[11.74T]}_{exp},R^{1[16.45T]}_{exp}]}(\tau_c,\theta_0) \propto g(R^{eff}_{1[11.74T]}[\tau_c,\theta_0], R^{exp}_{1[11.74T]}) \times g(R^{eff}_{1[16.45T]}[\tau_c,\theta_0], R^{exp}_{1[16.45T]}) \qquad (24)$$

where $R^{exp}_{1[B0]}$ is the R_1 measured at the field B_0, and $R^{eff}_{1[B0]}$ is the calculated effective relaxation rate determined in section 2. $P(\tau_c,\theta_0)$ measures the deviation between experimentally determined relaxation rates and the best fit for the determination of dynamic parameters.

The probability functions were evaluated for 29 residues in the protein Crh. For each residue, $P(\tau_c,\theta_0)$ is a combined function of the quality of the experimental data (i.e., the deviation in R_1), and the resolution with which a given dynamic behavior can be determined through the observation of a crossing of curves resulting from a relaxation measurement at two different fields. For 15 residues (V8, T12, G13, D38, G39, K41, K45, I47, G49, L50, M51, T57, I64, D69, Q82) we measure a rate and a cone angle with a reasonable accuracy. Diffusion times τ_w for these residues range from 5×10^{-8} s to 5×10^{-7} s, and the cone angle ranges from 5° to 20°. (We note at this stage that this corresponds to characteristic correlation times τ_0, $\tau_{\pm1}$, $\tau_{\pm2}$ of the exponential contributions to the overall correlation function of eq 4 having values ranging from 9×10^{-10} to 1.2×10^{-8} for τ_0, 1.7×10^{-9} to 5.7×10^{-8} for $\tau_{\pm1}$, and 6.2×10^{-10} to 2×10^{-8} for $\tau_{\pm2}$.)

To illustrate the analysis, we show three representative determined probability distributions in Figure 12. G39 (in a loop) and K41 (in a β sheet) are seen to have probability distributions that can be clearly easily distinguished. For K41, the cone angle is poorly defined, but the diffusion rate constant is well determined. We can also quite clearly distinguish between distributions obtained for D38 and G39, which have similar dynamics. The distributions for all residues are given in the Supporting Information. The results are summarized in Figure 13 that shows a bar graph of diffusion times and cone angles that were determined through the analysis of these probability

(27) http://www.ens-lyon.fr/CHIMIE/Fr/Groupes/NMR/Pages/library.html.
(28) De Paepe, G.; Elena, B.; Emsley, L. *J. Chem. Phys.* **2004**, *121* (7), 3165−3180.
(29) De Paepe, G.; Giraud, N.; Lesage, A.; Hodgkinson, P.; Böckmann, A.; Emsley, L. *J. Am. Chem. Soc.* **2003**, *125* (46), 13938−13939.
(30) De Paepe, G.; Hodgkinson, P.; Emsley, L. *Chem. Phys. Lett.* **2003**, *376* (3−4), 259−267.
(31) Galinier, A.; Haiech, J.; Kilhoffer, M. C.; Jaquinod, M.; Stulke, J.; Deutscher, J.; Martin-Verstraete, I. *Proc. Natl. Acad. Sci. U.S.A.* **1997**, *94*, 8439−8444.

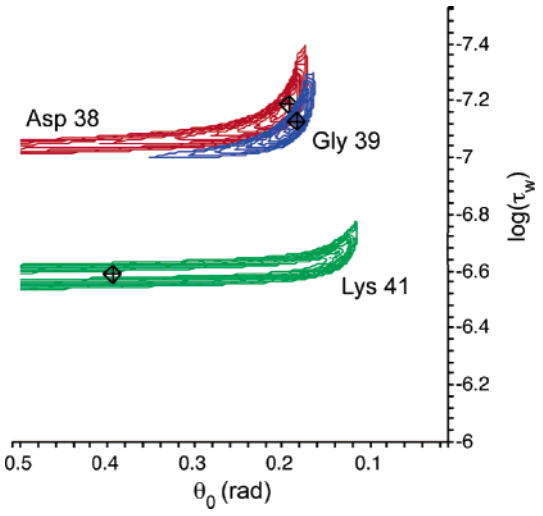

Figure 12. Contour plots of $P(\tau_c,\theta_0)$ for three residues :Asp 38 (red), Gly 39 (blue), and Lys 41 (dark green). (The relative vertical scales are indicated in the extended figure in the Supporting Information.)

contour plots. (The accuracy of each measurement, and the shape of the resulting dynamic distribution, can be estimated through direct observation of the contour plots in the Supporting Information.)

The observed variations from one site to another are coherent with the differential dynamic behavior that might be expected for the different secondary structures. In particular, in general, residues located in loops (V8, D38, G39, T57) have larger cone angles, whereas residues in helices and sheets (T12, G13, I47, G49, L50, M51, I64, Q82) have smaller cone angles. (Note that for the residue K41 in β-sheet, the rate is accurately determined, but the cone angle is not (see Figure 12)).

We note that residues located in loops, in particular D38, G39, and T57, also appear to have faster diffusion rate constants ($\tau_w < 1.7 \times 10^{-7}$ s), while residues in helices and sheets such as T12, G13, K41, G49, L50, M51, I64, and Q82 have slower diffusion times ($\tau_w > 1.7 \times 10^{-7}$ s).

Finally, we note that for some residues these data are not sufficiently accurate to determine dynamic parameters. This can be due to (i) the error in the measured T_1, (ii) the difference in relaxation rates between 500 and 700 MHz is not large enough to reliably constrain spectral densities, (iii) the simple diffusion in a cone model does not provide a correct description of the motion of the N−H vector, or (iv) deviations from the simple dipolar mechanism to describe longitudinal relaxation used here. This last point is particularly interesting. Obviously, the nitrogen-15 CSA is expected to make an increasingly significant contribution to relaxation as the field is increased, but there are several other possible mechanisms that could be invoked and that will need to be tested in the future; for example, cross relaxation to neighboring nuclei (first and foremost of which being the adjacent amide proton). Another source of relaxation that has recently been proposed for carbon-13 T_1 in solid proteins is due to paramagnetic oxygen that can be dissolved in the vicinity of the hydrophobic side chains, as postulated by Morecombe et al.[32] Having said this, for nitrogen-15 the NH dipolar coupling should logically be the dominant mechanism, and the other interactions will be perturbations to quantitative analysis.

All of these sources of error can be minimized. In the first case, for example, we can improve the sensitivity of the experiments, as well as the resolution of correlation peaks, for instance by using recoupling methods which would allow us to analyze N−CB correlations as well as N−CA. Moreover, we

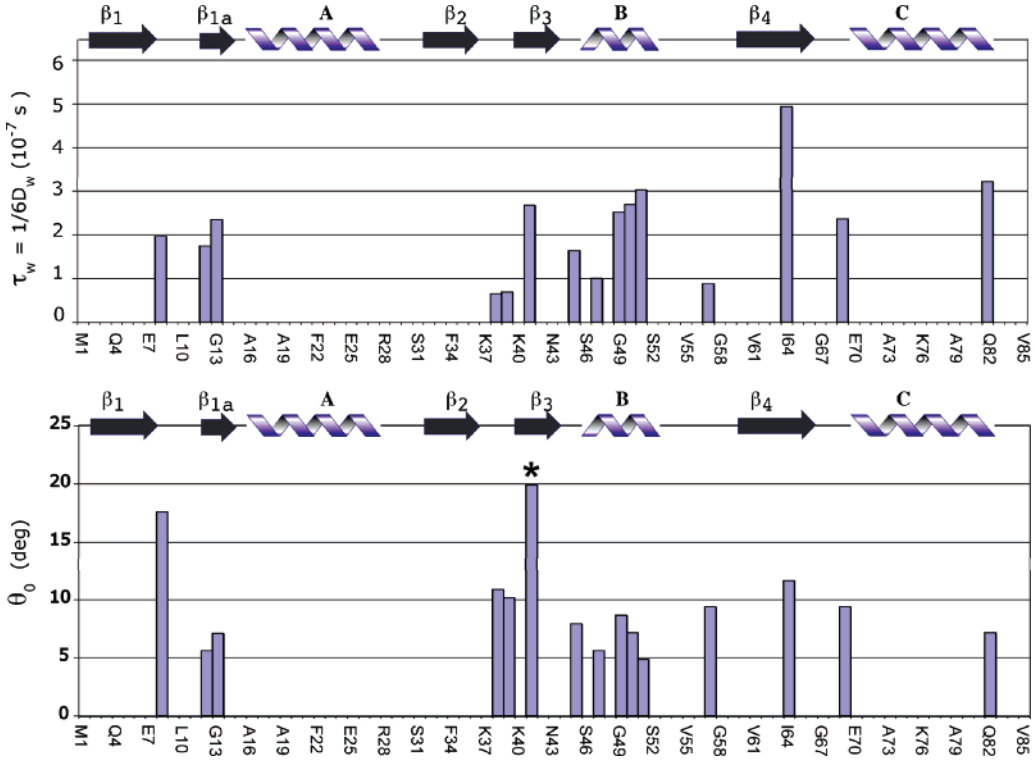

Figure 13. Bar graph for (above) τ_w and (below) θ_0 of the 15 best dynamic parameters determined through the analysis of nitrogen-15 longitudinal relaxation rates at two different fields (500 and 700 MHz), using the theoretical model described above. The asterisk on K41 indicates that for this residue the determination of θ_0 is unreliable (but τ_w is well determined).

can include quite straightforwardly the contribution of chemical shift anisotropy to the relaxation mechanism and use other relaxation measurements to constrain spectral densities such as, for example, $^{1}H-^{15}N$ cross-relaxation. Finally, we can evaluate the influence of other motional models on the quality of the determination of dynamic parameters. These avenues are under investigation in our laboratory.

6. Conclusions

In this paper we have presented a detailed analysis of nitrogen-15 longitudinal relaxation times in microcrystalline proteins. A theoretical model, based on and extending the model proposed by Torchia and Szabo,[11] is presented to quantitatively interpret relaxation times in terms of motional amplitude and characteristic time scale. Different averaging schemes were examined in order to propose an analysis of relaxation curves that takes into account the specificity of MAS experiments. In particular, it was shown that magic angle spinning averages the relaxation rate experienced by a single spin over one rotor period and that this results in individual relaxation curves that are dependent on the orientation of their corresponding carousel with respect to the rotor axis. Powder averaging thus leads to a *nonexponential behavior* in the observed decay curves.

We showed how to extract dynamic information from experimental decay curves and illustrated this using a diffusion in a cone model. Obviously the method and conclusions presented here can be extended to other motional models, possibly better describing internal motion in these samples. We can also develop expressions for other relaxation mechanisms, notably to include the effect of nitrogen-15 CSA. The method applies equally to the interpretation of deuterium relaxation measurements,[15,17] which has traditionally been used as a probe of dynamics in deuterium labeled proteins.[10,16,33,34] Notably, the approach to measuring internal dynamics in proteins is of great interest as a complementary method to both solution state NMR and diffraction methods. In particular, relaxation studies in solution are complicated by the superposition of internal motions and overall tumbling, whereas in solid proteins only the internal motion is present to contribute to relaxation.

We have applied this approach to the study of spin−lattice relaxation rates measured at 11.74 and 16.45 T for the microcrystalline protein Crh and have been able to determine differential dynamic parameters for several residues in the protein. Notably we observe generally smaller amplitude motions for secondary structures, as may be expected. We also observe slower diffusion rate constants for residues in helices and sheets than those in loop structures. The data and analysis we present here clearly demonstrate that this is a viable method of determining dynamics in crystalline proteins.

Supporting Information Available: ^{15}N longitudinal relaxation rates (R_1) measured for the different residues in microcrystalline Crh at 11.74[12] and 16.45 T, and an estimation of the standard deviation of each rate. Contour plots of the "χ^2" surfaces $P(\tau_c,\theta_0)$, as well as contours plots of the dynamic parameters determined from the relaxation rates measured at two different fields. Dynamic parameters extracted from the ^{15}N longitudinal relaxation rates for the different residues in microcrystalline Crh. Numerical values for c_{ij}^{λ} coefficients calculated with Maple software in order to evaluate $C_{ij}^{MAS}(\beta_1)$. This material is available free of charge via the Internet at http://pubs.acs.org.

JA055182H

(32) Morcombe, C. R.; Gaponenko, V.; Byrd, R. A.; Zilm, K. W. *J. Am. Chem. Soc.* **2005**, *127* (1), 397−404.
(33) Rozovsky, S.; McDermott, A. E. *J. Mol. Biol.* **2001**, *310* (1), 259−270.
(34) Hologne, M.; Faelber, K.; Diehl, A.; Reif, B. *J. Am. Chem. Soc.* **2005**, *127* (32), 11208−11209.